Interface and transport properties of Fe/V/MgO/Fe and Fe/V/Fe/MgO/Fe magnetic tunneling junctions

Xiaobing Feng,[1] O. Bengone,[1] M. Alouani,[1] I. Rungger,[2] and S. Sanvito[2]
[1]*Institut de Physique et Chimie des Matériaux de Strasbourg, CNRS–UdS, UMR 7504, 23 rue du Loess, 67034 Strasbourg Cedex, France*
[2]*School of Physics and CRANN, Trinity College, Dublin 2, Ireland*
(Received 26 February 2009; revised manuscript received 28 April 2009; published 25 June 2009)

The interface and transport properties of Fe/V/MgO/Fe and Fe/V/Fe/MgO/Fe magnetic tunneling junctions are investigated by using density-functional theory and nonequilibrium Green's-function methods. Bader analysis reveals that the Fe layer at the interface with MgO loses a small amount of charge with respect to its bulk value, in contrast to a previous study [W. H. Butler, X.-G. Zhang, T. C. Schulthess, and J. M. MacLaren Phys, Rev. B **63**, 054416 (2001)]. At the same time at the Fe/V interface a magnetic moment is induced on the V layer by proximity. Importantly, the direction of the magnetization of the first V monolayer immediately close to the MgO barrier oscillates with the total V-layer thickness and the relative stability of a particular magnetic configuration weakens as such a thickness is increased. These two aspects pose a challenge to the Fe/V/MgO/Fe device signal stability. A more intriguing situation is found for Fe/V/Fe/MgO/Fe junctions. Their transport properties depend sensitively on the thickness of the Fe layer intercalated between V and the MgO barrier. This is the result of resonances through quantum-well states of Δ_1 symmetry localized in the intercalated Fe layer. In particular, for some geometries we find a massive magnetoresistance obtained by simply switching the direction of the magnetization of the Fe interlayer, while keeping the direction of the electrodes fixed. This effect may be employed in the design of new spin valves with extremely high spin polarization but still relatively large current densities.

DOI: 10.1103/PhysRevB.79.214432 PACS number(s): 71.15.Ap, 71.20.Eh

I. INTRODUCTION

Magnetic tunneling junctions (MTJs), consisting of metallic magnetic electrodes separated by insulating or semiconducting materials, have been intensively studied since a pronounced giant magnetoresistance effect[1,2] was discovered in these junctions. Such MTJs have applications in sensors, data storage, and magnetic random access memory, and presently most of the technology behind hard disk read heads is based on MTJs. The first MTJs were based on amorphous Al_2O_3 barriers. In this case, the tunneling magnetoresistance (TMR) can be explained by the Julliere model,[3] where the only parameter determining the TMR is the spin polarization of the density of states (DOS) of the magnetic electrodes.[4,5] In fact, for amorphous insulators the tunneling barrier simply determines the magnitude of the tunnel current but not its spin polarization.

A different situation is encountered for crystalline barriers. *Ab initio* calculations predicted first a large TMR for perfectly epitaxial Fe/MgO/Fe MTJs,[6] pointing out the importance of describing the detailed electronic structure of both the barrier and the electrodes.[7] The fundamental concept in this case is that electrons with different wave-function symmetry experience different effective barrier heights when tunneling through a crystalline insulator.[6] In the particular case of Fe/MgO, the wave function of electrons with Δ_1 symmetry has a much slower decay across the MgO barrier than that of any other symmetry. Since the spin split of the Δ_1 band is such that only one spin direction is present at the Fe Fermi level (E_F), the Fe/MgO system effectively behaves as a half metal, at least if the MgO barrier is large enough. Such a symmetry-filtering effect leads to a much larger TMR than that obtained with Al_2O_3-based junctions, for which the limiting factor is the spin polarization of Fe. This prediction was than later confirmed by experiments.[8] Based on the same symmetry-filtering concept, even larger TMRs have been predicted for MTJs using bcc Co and FeCo electrodes.[9]

An important aspect, when comparing theory with experiments, is that usually the theoretically predicted TMRs are much larger than those observed experimentally. In addition to the difficulty in theoretically dealing with interface states, the disagreements are often attributed to imperfections in the MTJ junctions such as Fe oxidation at the Fe/MgO interface and dislocations caused by the lattice-constant mismatch. Interestingly, improvements in the deposition techniques and thus in the junction quality have greatly enhanced the experimentally measured TMR,[10–12] bringing it closer to the predicted value. Usually the magnitude of the TMR is measured by "optimistic" TMR ratio

$$\mathrm{TMR}^{\mathrm{opt}} = \frac{I_{\mathrm{P}} - I_{\mathrm{AP}}}{(I_\alpha)^{\mathrm{min}}}, \tag{1}$$

where I_{P} is the total current in the parallel (P) configuration of the device, I_{AP} is the total current in the antiparallel (AP) configuration, and $(I_\alpha)^{\mathrm{min}}$ is the smallest of the two. According to this definition, TMR as high as 1010% at 5 K and 500% at room temperature has been found in MgO-based junctions using $(Co_{25}Fe_{75})_{80}B_{20}$ as electrodes.[13] Other definitions which would also be used in this study are the pessimistic TMR definition

$$\mathrm{TMR}^{\mathrm{pes}} = \frac{I_{\mathrm{P}} - I_{\mathrm{AP}}}{(I_\alpha)^{\mathrm{max}}}, \tag{2}$$

where $(I_\alpha)^{\mathrm{max}}$ is the largest between I_{P} and I_{AP} and the "normalized" definition

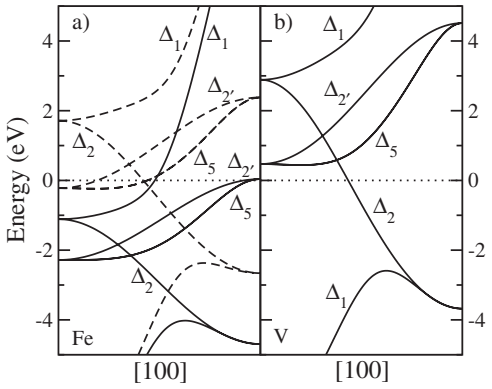

FIG. 1. Band structure along the [100] direction of bulk bcc Fe (panel a) and bcc V (panel b). The solid and dashed lines in the left panel represent the energy bands of majority and minority spins, respectively.

$$\mathrm{TMR}^{\mathrm{nor}} = \frac{I_{\mathrm{P}} - I_{\mathrm{AP}}}{I_{\mathrm{AP}} + I_{\mathrm{P}}}. \tag{3}$$

Another fruitful line of investigation consists in inserting either magnetic [e.g., Cr (Refs. 8 and 14)] or nonmagnetic [e.g., Cu (Ref. 15) and Ag (Ref. 16)] layers at the electrode/barrier interface. This has effects over the symmetry filtering and the formation of both interface[16] and quantum-well states.[8] In practice, such insertion can also be used for improving the crystal orientation of polycrystalline MgO leading to low resistance and high TMR ratio.[17]

In this work, the interfacial and transport properties of Fe/V/MgO/Fe and Fe/V/Fe/MgO/Fe MTJs are investigated by using the *ab initio* nonequilibrium Green's-functions (NEGF) method implemented in the SMEAGOL code.[18–20] The choice of vanadium is dictated by the fact that, at variance with other transition metals, V is nonmagnetic but it can be easily polarized by proximity with a magnetic material. As a consequence, our results show that the magnetic configuration of the V layer at the Fe/MgO interface is sensitive in its thickness. Another interesting feature of V comes from its wave-function symmetry at E_{F}. As shown in Fig. 1, there is only one band of Δ_2 symmetry crossing the Fermi energy in the [100] direction, with the two Δ_1 bands positioned at around 3 eV both above and below E_{F}. Finally the Δ_5 band, which rapidly decays across MgO, is about 0.5 eV above E_{F}. It is then expected that at zero bias, the V layer could provide an additional potential barrier with effective barrier height higher than that of Cr.[8] Furthermore significant changes in conductance are expected when the bias is increased to a point (0.5 V), where the Δ_5 band enters into the bias window. Our results confirm these conjectures and show a dramatic reduction in the conductance as the V layer is inserted at the Fe/MgO interface. Furthermore, conductance oscillations with increasing the number of V monolayers are observed. These correlate with the oscillations of the magnetization of the interface V ions. Finally, when an additional Fe layer is inserted between V and MgO, thus forming a Fe/V/Fe/MgO/Fe MTJ, quantum-well states of Δ_1 symmetry are created in the intercalated Fe layer and affect sensitively the electronic transport.

The paper is organized as follows. We start in Sec. II with presenting the computational details, followed by the discussion of the interface properties of both Fe/MgO/Fe and Fe/V/MgO/Fe MTJ in Sec. III. Then the transport properties of Fe/V/MgO/Fe and Fe/V/Fe/MgO/Fe MTJs are presented in Secs. IV A and IV B, respectively. Finally we draw our conclusions in Sec. V.

II. COMPUTATIONAL DETAILS

Transport calculations are carried out in the elastic limit, in which the tunneling current, I, can be calculated by using the Landauer-Büttiker formula,[21–23]

$$I = \frac{e^2}{h}\int dE\, T(E)[f(E-\mu_{\mathrm{L}}) - f(E-\mu_{\mathrm{R}})], \tag{4}$$

where $T(E)$ is the energy- and bias-dependent transmission coefficient, f is the Fermi distribution function, and μ_{L} (μ_{R}) is the chemical potential of left-hand (right-hand) side electrode. Finite bias is introduced as a shift of the chemical potentials $eV=\mu_{\mathrm{L}}-\mu_{\mathrm{R}}$ deep into the bulk of the electrodes with the potential drop at the junction being calculated using the NEGF prescription.[24–28] At zero bias, the conductance is given by $\frac{e^2}{h}T(E_{\mathrm{F}})$, i.e., it is proportional to the transmission coefficient at the Fermi energy. For coherent tunneling, the electron spin and the momentum parallel to the interface are both conserved, thus $T(E)$ can be written as a sum over the momentum and spin-resolved transmission coefficient, $T^{\sigma}(E,\mathbf{k}_{\parallel})$, as

$$T(E) = \sum_{\sigma,\mathbf{k}_{\parallel}} T^{\sigma}(E,\mathbf{k}_{\parallel}), \tag{5}$$

where σ is the spin index and $\mathbf{k}_{\parallel}$ is the parallel (to the interface) component of the wave vector of a tunneling electron. The NEGF formalism for transport,[24–28] combined with density-functional theory (DFT) and implemented in SMEAGOL,[18–20] is used here to calculate the transmission coefficients. The PBE generalized gradient approximation (GGA) for the exchange-correlation potential is employed.[29]

Troullier-Martins norm-conserving nonrelativistic and nonlocal pseudopotentials (PPs) are used for Fe, Mg, O, and V. The atomic configurations for generating the PPs are $4s^1 3d^7$, $3s^2$, $2s^2 2p^4$, and $4s^2 3d^3$, respectively. The cutoff radii (in atomic units) for s, p, and d orbitals of Fe, Mg, and O are 2.0, 2.59, and 1.14, respectively. The cutoff radii of the V PP are 2.56 for s and p orbitals and 0.73 for d orbitals. Nonlinear core corrections are used for Fe, Mg, and V.

The *ab initio* engine behind SMEAGOL is the numerical implementation of DFT contained in the SIESTA code,[30,31] which uses finite-ranged numerical orbitals as basis set. Split-valence bases for Mg and O are of double zeta type for s and p orbitals with the largest cutoff radii being 6.0 a.u. For Fe and V, the same type of basis is used: double zeta for $4s$ and single zeta for $4p$ and $3d$ orbitals with cutoff radii 5.6 a.u. for $4s$ and $4p$ and 5.2 a.u. for $3d$ orbitals. For V, the cutoff radii are 6.0 a.u. The default energy shift is employed to determine the cutoff radii of the second zetas. The electronic temperature is 300 K. A mesh cutoff of 600 Ry, which

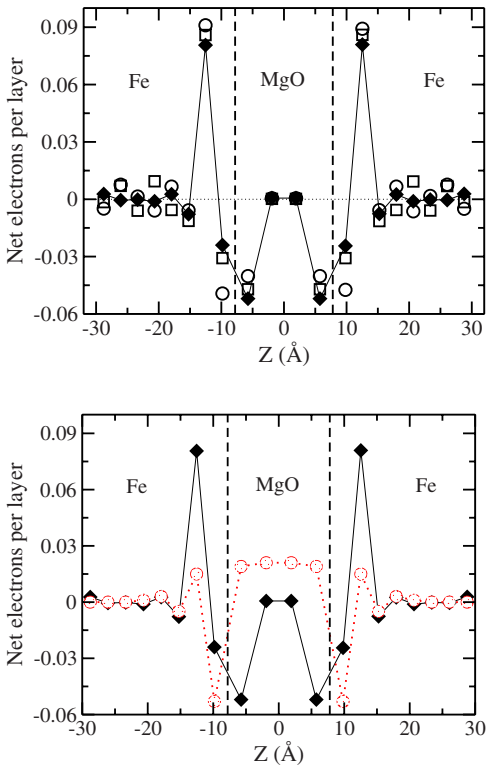

FIG. 2. (Color online) (Top panel) Charge transfer at the Fe/MgO interface as calculated from the Bader analysis based on the SIESTA PBE GGA charge densities. The junction is made of four layers of MgO and 16 layers of Fe. Periodic boundary conditions are used in all directions. Three different real-space grids $72\times72\times750$ (open circle), $96\times96\times1080$ (open square), and $120\times120\times1250$ (solid diamond), are used to monitor convergence. (Bottom panel) Charge transfer at the Fe/MgO interface as calculated using the SIESTA code from the most converged Bader analysis (black squares) compared to the Mulliken analysis (red circles). The Fe/MgO interface is the same as in the top panel.

specifies the real-space grid for defining the potential and the electron density, is used. In this work the structural parameters of Fe/MgO/Fe junctions are same as those in Ref. 6. The structure of Fe/V/MgO/Fe is generated from Fe/MgO/Fe junctions by replacing a few Fe layers of the left electrode with V. Further structural relaxation and its effects are not considered in this work.

III. RESULTS AND DISCUSSION

A. Charge transfer and magnetic moment at the Fe/MgO interface

The electronic transport properties of Fe/MgO-based MTJs depend not only on the electronic structures of bulk Fe and MgO but also on the structure and electronic states of the Fe/MgO interface. Two basic quantities, charge transfer and magnetic moment, are studied using Bader analysis.[32–34] This method is based on the real-space charge density and is thus independent of choice of basis functions in the DFT calculations.

In the top panel of Fig. 2, we present the charge excess

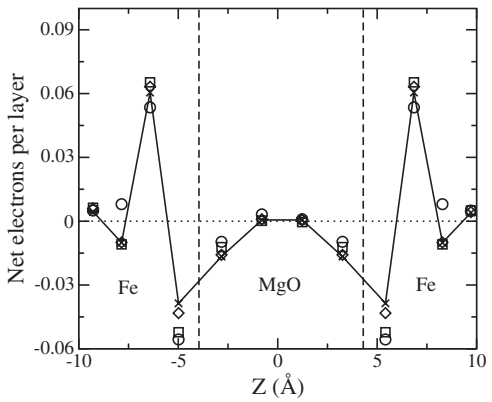

FIG. 3. Charge transfer at the Fe/MgO interface as calculated from the Bader analysis based on the VASP LDA charge densities. The junction is made of four layers of MgO and eight layers of Fe. Periodic boundary conditions are applied in all directions. Four different real-space grids $48\times48\times336$ (circle), $96\times96\times672$ (square), $192\times192\times1344$ (diamond), and $300\times300\times2100$ (cross) are used to monitor the convergence.

over the bulk values as a function of the position along the layer stack as calculated from SIESTA (positive charge means electron excess). The figure shows that the charge transfer is rather confined to the interface region, already being very small beyond the second Fe and first MgO layers. We find that the Fe atoms next to the MgO and the first MgO layer lose electrons, which are moved to negatively charge the second Fe monolayer from the interface. Such charge-transfer pattern is different from what is previously reported,[6,35] where the interface Fe layer had an excess of 0.1 electrons over the Fe bulk value. The disagreement could be due to the fact that they have used an atomic-sphere approximation, i.e., the potential and the charge density are spherical and none of the spherical components are neglected. To investigate further the charge transfer at the interface, we have also compared in bottom panel of Fig. 2 the charge transfer produced using the most converged Bader analysis with the basis-dependent Mulliken analysis. We can notice from the figure that the agreement is only qualitative at the interface. The Mulliken analysis shows that all MgO layers acquire some electronic charge, whereas the first Fe layer loses more charge and the second Fe layer gains less charge than in the Bader analysis. We could of course debate which type of charge-transfer analysis is more accurate. In our view there is no clear answer to such a question. The only argument in favor of Bader analysis is that it is independent of the type of basis set used in the calculation as it is also shown using the plane-wave basis set in the next paragraph.

Since these published results are in contrast to our calculations, in order to check the reliability of the Bader analysis based on the SIESTA charge density, we repeat the same analysis by using the charge density generated with the plane-wave DFT code VASP.[36–39] In this case the projected augmented wave (PAW) method,[40,41] the local-density approximation (LDA) functional[42] are used and the results are presented in Fig. 3. Clearly there is a good qualitative agreement between our two calculations with the remaining differences being attributed to the different DFT functionals

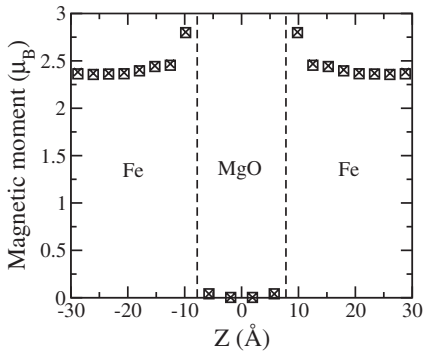

FIG. 4. Magnetic-moment profile across the Fe/MgO/Fe junction and obtained from Bader analysis using SIESTA PBE GGA charge and spin densities. The junction is made of four layers of MgO and 16 layers of Fe. Two different real-space grids, i.e., $72\times72\times750$ (square) and $120\times120\times1250$ (cross), are used to monitor the convergence.

used (GGA versus LDA). We note that such transfer of electrons from MgO to metals is also found in other systems. For example, Bader analysis of charge transfer at Rh/MgO interfaces indicates that there are 0.19 electrons transferred from MgO to Rh for one monolayer coverage.[43]

It is well known that at surfaces or interfaces, the magnetic moments of transition-metal elements can be significantly altered due to the lower coordination with the same kind of magnetic atoms. This is also true for the Fe/MgO interface. Shown in Figs. 4 and 5 are the magnetic moments calculated by integrating the spin densities over the Bader volume determined by the total charge densities from SIESTA GGA and VASP LDA calculations. These results are again qualitatively similar; the Fe magnetic moment is significantly enhanced at the Fe/MgO interfaces. We find a maximum magnetic moment of $2.70\mu_B$ and $2.80\mu_B$ for VASP and SIESTA, respectively. These magnetic moments at the interfaces are around 20% higher than those in the bulk.

B. Interface magnetic configuration of Fe/V/MgO/Fe junctions

Vanadium is a nonmagnetic metal with a large magnetic susceptibility so that a magnetic moment can be easily induced by proximity. The magnetic configuration of such induced magnetic V layer with respect to their neighbors however can depend sensitively over the details of the electronic structure. For instance, in Fe/V/MgO/Fe junctions, metastable states with different magnetic configurations of the V layers can be obtained. We investigate these configurations here with the aim of finding the lowest total-energy state to be used in the transport calculations. Previous calculations have shown that at the Fe/V interface, the nearest Fe and V monolayers are always antiferromagnetically coupled to each other.[44,45] This is also confirmed by our own results that show an energy gain of about 0.1 eV when changing the orientation of the Fe and V magnetic moments from parallel to antiparallel (note that throughout the paper we report value of energy normalized to the number of atoms at the interface). Therefore, in the search for the ground-state configuration of a given MTJ, the spin of the V ions immediately next to a Fe electrode is always kept antiparallel to that of Fe. Since we are only interested in determining the stable magnetic configurations and not in the quantitative predictions of the magnetic moments, the magnetic moments reported in this subsection are taken directly from the Mulliken population and not from the more accurate (but also more computationally demanding) Bader analysis.

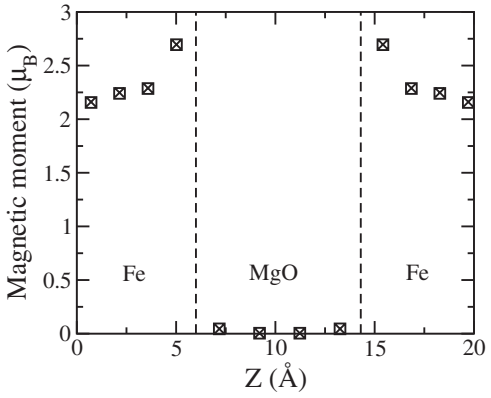

FIG. 5. Magnetic-moment profile across the Fe/MgO/Fe junction and obtained from Bader analysis using VASP LDA charge and spin densities. The junction is made of four layers of MgO and eight layers of Fe. The results shown are for two different real-space grids, i.e., $192\times192\times1344$ (square) and $300\times300\times2100$ (cross).

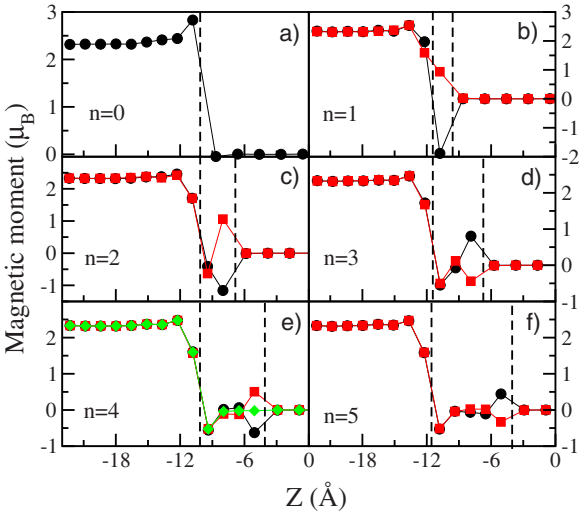

FIG. 6. (Color online) Magnetic-moment profile across $Fe/V_n/MgO/Fe$ junctions with a variable number of V monolayers. The junction consists of six MgO monolayers and either 18 or 17 Fe monolayers depending on whether n is even or odd. The magnetic moments are calculated using Mulliken analysis. The configurations with lowest energies are always depicted by using black solid circles while the metastable magnetic configurations are represented by red squares and green diamonds.

In Fig. 6 we present the magnetic-moment profile across a $Fe/V_n/MgO/Fe$ junction for various possible magnetic configurations and in which the V layer comprises a number of monolayers n ranging from 1 to 5. In the figure, the ground-state configurations are all labeled with black solid cycles. In general, the energy difference between competing configurations decreases with increasing the number of V monolayers. In the case where the V layer consists of only one single monolayer [$n=1$, see Fig. 6(b)], the total energy of the $\downarrow$

configuration is 104 meV smaller than that of the ↑ configuration. Here we have used the notation in which a V monolayer is in the ↓ (↑) configuration, if its local magnetic moment is antiparallel (parallel) to that of the left-hand side Fe electrodes. For $n>1$, the competing configurations are characterized by having the V monolayer next to Fe always ↓ and the last monolayer (the one close to MgO) being either ↑ or ↓. Thus the configuration where the last V monolayer is ↓ is energetically favored for $n=2$ and $n=4$ by, respectively, 34 meV and 13 meV over the one in which the last V monolayer is ↑. In contrast, for $n=3$ and $n=5$ the situation is reversed with energy differences of 45 meV and 4 meV, respectively, in favor of the ↑ configuration. This means that the ground-state configuration of the junction shows an oscillatory behavior of the magnetic moment of the V monolayer close to the MgO barrier as a function of the total V layer thickness. Notably, the induced magnetic moment in V at the V/MgO interface is comparable to or larger than that at the Fe/V interface and it is also different from the very small magnetic moment of a single V monolayer predicted for the Fe/V/vacuum structures.[44]

From Fig. 6, one can also observe that the magnetic moment of the Fe ions next to V is reduced and that in general it varies with the number of V monolayers. This deceases from about $2\mu_B$ for $n=1$ to $1.5\mu_B$ for $n=4$. The same sensitive dependence of the total magnetic moment of the interfacial layer at the Fe/V interface is reported for V. Thus the magnetic moment of the V next to Fe changes from $2\mu_B$ ($n=1$) to $0.5\mu_B$ ($n=4$). Finally we note that the induced magnetic moment on V decays rapidly away from the interfaces with the second V monolayer nearest to the Fe or MgO always having very small induced moment. These findings are in agreement with our previous study of the Fe/V/Fe interface.[45]

IV. TRANSPORT PROPERTIES OF FE/V/MGO/FE AND FE/V/FE/MGO/FE MTJS

A. Transport properties of Fe/V/MgO/Fe junctions

The effects of inserting a V layer close to the MgO barrier in the stack of Fe/MgO/Fe junctions over the transport properties are now investigated. We consider $Fe/V_n/MgO/Fe$ MTJs where the MgO thickness is kept constant at six atomic layers and that of V, n, is varied between 1 and 5 monolayers. In addition, the simulation cell also includes 18 Fe monolayers (for even n, 17 if n is odd). In order to facilitate the discussion, we define the spin subbands of the entire junction in terms of the spin subbands of the left-hand side Fe electrode (the one where the V layer is intercalated). The spin-resolved transmission coefficients at zero bias are presented in Fig. 7, where in panel (a) we report data for the case where no V layer is present. For such Fe/MgO/Fe MTJ, we observe a considerably larger transmission coefficient for the parallel configuration of the electrodes at all energies. In particular, the majority-spin component dominates the transmission except for a 0.1 eV wide region around E_F, where there is a large peak in the minority subband attributed to an interface state at the Fe/MgO interface. This is in substantial agreement with our previous calculations.[46–48]

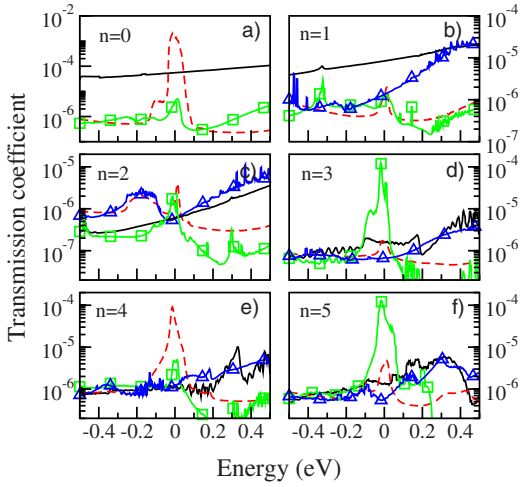

FIG. 7. (Color online) The energy-dependent spin-resolved transmission coefficients of $Fe/V_n/MgO/Fe$ MTJs at zero bias. The integer n in the panels represents the number of V monolayers inserted between Fe and MgO. The spin-resolved energy- and bias-dependent transmission coefficients are as follows: parallel-configuration majority spin (solid black line); parallel-configuration minority spin (dashed red line); antiparallel-configuration majority spin (solid green line with squares); antiparallel-configuration minority spin (solid blue line with triangles). For the antiparallel configuration, the spin direction is determined with respect to the left-hand side electrode.

Interestingly, as shown in Fig. 7(b), even a single V monolayer dramatically reduces the transmission coefficients of all spin channels and at all energies. Although the interface state can still be seen for the minority spins in the parallel configuration, its magnitude is significantly reduced with respect to the $n=0$ case, leading to a contribution to the total transmission smaller than that of the majority spins. In contrast, in the antiparallel configuration, the most notable feature is the spin-degeneracy breaking due to the loss of inversion symmetry of the entire device. In general, however, the transmission in the antiparallel configuration still remains considerably lower than that of the parallel one, giving rise to a positive magnetoresistance.

The situation for $n>1$ becomes more complicated. In general all spin-resolved transmission coefficients are further reduced for $n=2$ with the reduction being more severe for the majority-spin channel in the parallel configuration. At larger thicknesses, oscillations as a function of n appears in the transmission. In particular, this is evident in the energy region around E_F, where pronounced transmission peaks rise for the majority spins in the antiparallel configuration ($n=3$ and $n=5$) and for the minority spins in the parallel one ($n=2$ and $n=4$). Since these peaks entirely dominate $T(E_F)$, the zero-bias transmission is expected to be an oscillating function of the V thickness with a period of only 2 monolayers. Furthermore, for $n=3$ and $n=5$ the conductance in the antiparallel configuration is larger than that of the parallel one and the TMR becomes negative.

These conductance oscillations, as a function of the V layer thickness, are presented in Fig. 8 where we show $T(E_F)$ as a function of n for all the spin channels. The figure con-

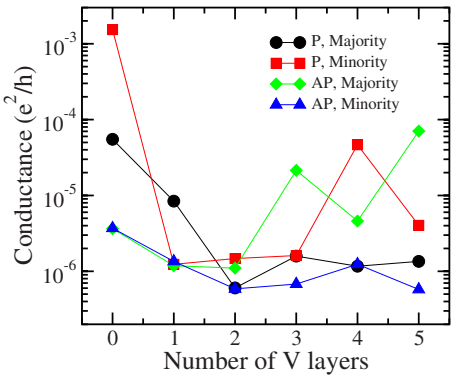

FIG. 8. (Color online) Dependence of the zero-bias conductance of $Fe/V_n/MgO/Fe$ on the number, n, of V monolayers. The majority-spin and minority-spin conductances are denoted with circles and squares, respectively, for the P configuration of the Fe electrodes and with diamonds and triangles for the AP configuration. The conductance shows clear oscillations with increasing number of V layers.

firms our previous discussion and shows that the period of oscillations is indeed of two monolayers. In particular, the conductance for the majority-spin channel of both parallel- and antiparallel-configurations peaks at odd n, while that of the minority-spin channels (for both the device configurations) peaks at even n. Such a behavior can be understood by recalling the fact that the direction of the induced magnetization of V monolayer next to the MgO barrier oscillates with n (see discussion in Sec. III B). In particular, it is parallel to the magnetization of the left-hand side Fe electrode for odd n and antiparallel for even n. Such oscillation in the magnetic-moment orientation correlates well with the conductance oscillations. This means that the orientation of the magnetic moment of the V monolayer next to the MgO barrier has a large influence on the transmission, with electrons having high transmission probabilities when their spins are parallel to the magnetization of the V and low transmission when they are antiparallel.

As expected, conductance oscillations generate oscillations in the TMR, as displayed in Fig. 9. In this figure, we present the data by using three alternative definitions of

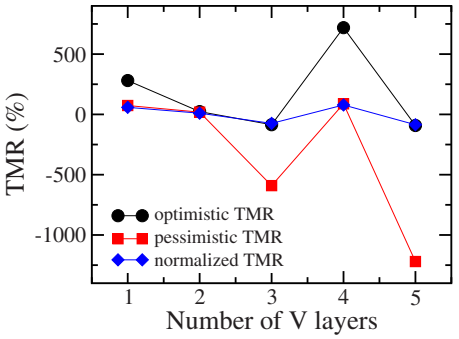

FIG. 9. (Color online) Dependence of the TMR of $Fe/V_n/MgO/Fe$ MTJs over n according to the different TMR definitions: optimistic (black circles), pessimistic (red squares), and normalized (blue diamonds). The conductances show clear oscillations with increasing the number of V monolayers for $n>1$.

TMR depending upon the normalization condition used to normalize the difference between the currents in the two device configurations. Thus, in addition to the optimistic definition of Eq. (1), we use the "pessimistic" definition and the normalized definition as given by Eq. (3) Note that at low bias, in the linear-response limit, the currents can be replaced by the conductance or alternatively with $T(E_F)$. The oscillations in the TMR are present for all the definitions although they are certainly more pronounced for the optimistic and pessimistic one. Also note that for all the definitions, the TMR assumes negative values.

Whether or not one will be able to observe these conduction oscillations depend on the magnetic stability of the MTJ. Unfortunately our total-energy calculations presented in Sec. III B demonstrate that as the thickness of the V layer is increased, the total energies of magnetic configurations differing for the different orientation of the V monolayer next to the MgO barrier become very similar. This means that thermal fluctuations will make the orientation of such terminal V monolayer unstable. Since the magnitude of the various spin currents is critically dependent on the magnetic configuration of the V layer, we expect a growing device instability as its thickness is increased.

The spin- and k-resolved transmission coefficients at E_F, $T^\sigma(E_F,\mathbf{k}_\parallel)$ of Eq. (5), are shown in Fig. 10 and help in understanding how the bands symmetry affects the transport. We observe two main features. First of all, as V is introduced in the MTJ, there is a dramatic reduction in the transmission of the majority spins in the parallel configuration primarily due to a strong suppression of $T^\sigma(E_F,\mathbf{k}_\parallel)$ in the middle of the two-dimensional Brillouin zone (2D BZ). This is expected by looking at the band symmetry of both Fe and V (see Fig. 1). In fact the Δ_1 band, present at E_F for the majority spins and dominating the transmission at the 2D BZ center, is absent in bulk V. Thus the effect of the V layer is that of suppressing the majority Δ_1 transmission. The second notable effect is the general relative increase in transmission for all spins in all configurations at the 2D BZ edges as compared to that in other portion of the 2D BZ. This is related to the transmission through both the Δ_2 and Δ_5 bands which are present at E_F for both Fe and V. Finally we wish to point out the suppression of transmission in the minority spins for the parallel configuration originating from the portion of the 2D BZ next to its center. This is the region dominated by the Fe/MgO surface state, which indeed is not present once a V layer is intercalated at the interface.

Next, the spin- and k-resolved projected density of states (PDOS) at E_F for the V interface layer immediately next to the MgO barrier is shown in Fig. 11. Although this is not indicative of the transport properties since electrons with different linear momentum may experience different effective barrier heights, the k-resolved PDOS can still provide some valuable information to our analysis. From the figure, one can notice that a single V layer dramatically reduces the minority-spin PDOS over the entire 2D BZ. Likewise, there is a strong reduction in PDOS at the 2D BZ center when going from $n=0$ to $n=1$ and then again from $n=1$ to $n=2$. These all correlate well with the suppression of the conductance for the relative spin channels. Another feature worth noticing is the oscillation of the PDOS as a function of n

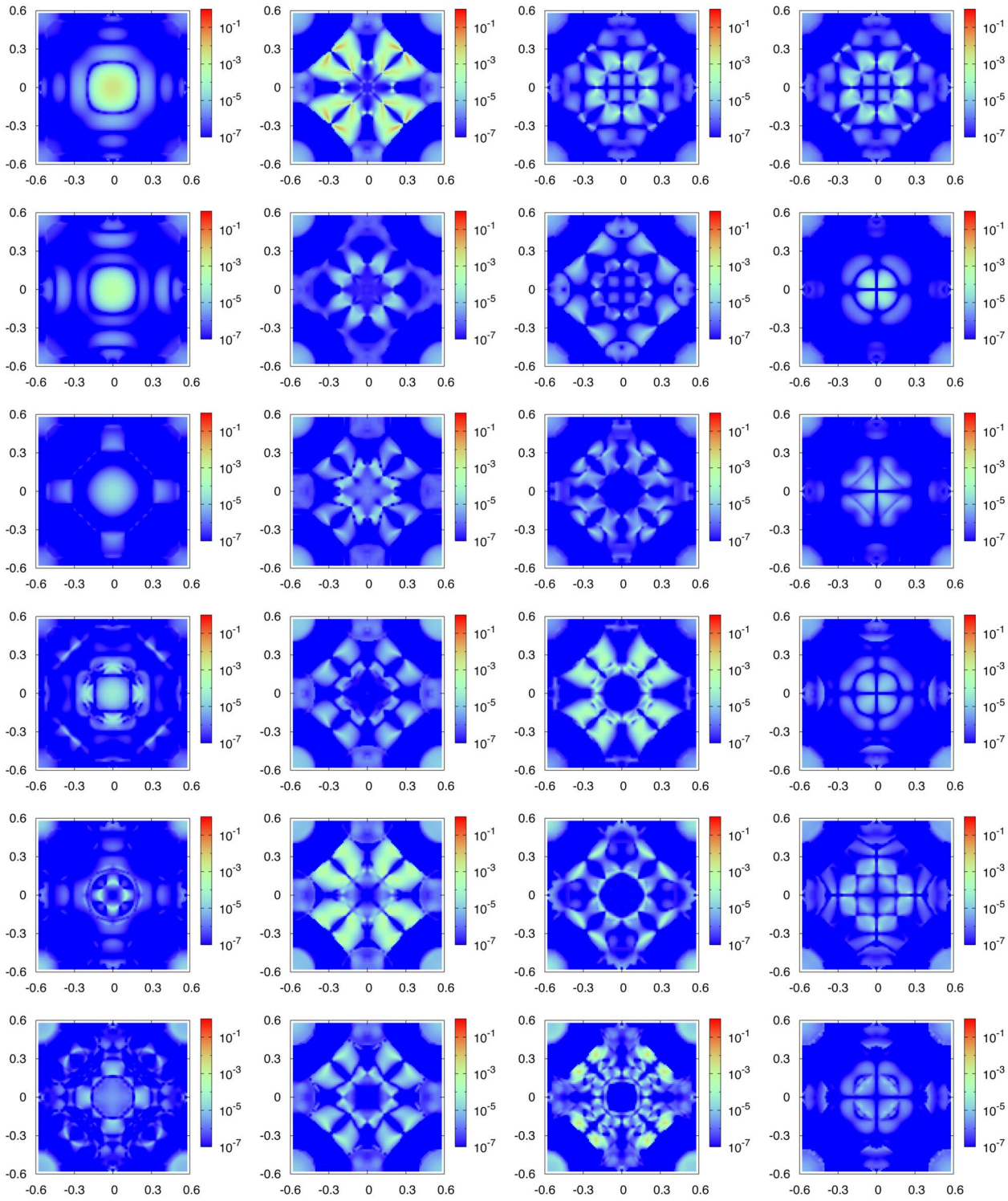

FIG. 10. (Color online) The k-resolved transmission coefficients of Fe/V/MgO/Fe MTJs. Panels from left to right are, respectively, for P-configuration majority spins, P-configuration minority spins, AP-configuration majority spins, and AP-configuration minority spins. Panels from top to bottom show results for Fe/V_n/MgO/Fe MTJs for different n, with $n=0$ at the top and $n=5$ at the bottom.

connected with the oscillation of the last V layer magnetization. Thus the PDOS for both the spin channels of the $n=2$ MTJ is rather similar to that of $n=4$. Similarly, the PDOS of $n=3$ resembles closely to that of $n=5$. Finally one can also observe that the PDOS of the $n=4$ MTJ is actually similar to that of both $n=5$ and $n=3$ once the spin channels are exchanged. This is expected from the oscillating behavior of the magnetization of the terminating V monolayer, as discussed in the previous section.

Finally, in order to correlate the conductance oscillations to the electronic structure, the PDOS of the 3d orbitals of the V($n>0$) and Fe($n=0$) layer immediately next to the MgO

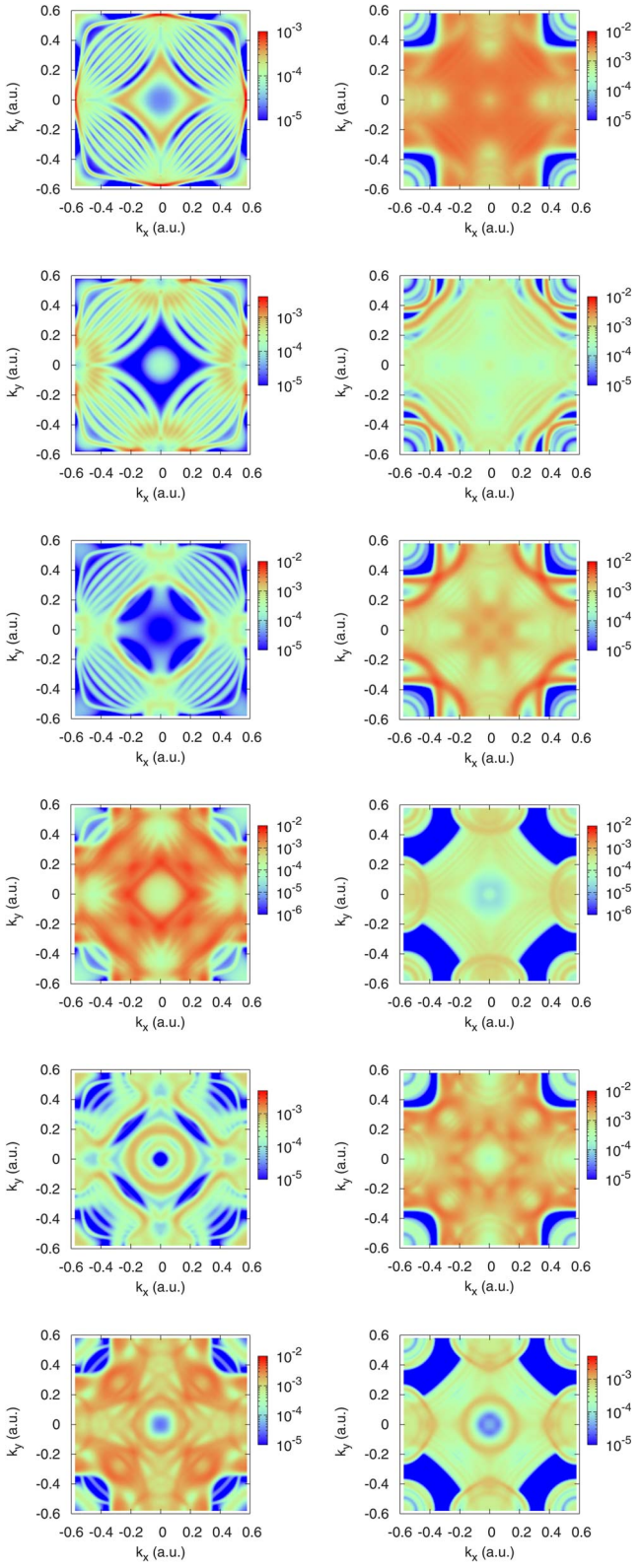

FIG. 11. (Color online) The spin- and k-resolved projected density of states of the interface layer immediately next to the MgO barrier in Fe/V_n/MgO/Fe MTJs. The left and right panels are for majority and minority spins, respectively. Vertically we display results for increasing n from $n=0$ (top panels) to $n=5$ (bottom panels). In the case of $n=0$ the layer is made of Fe, while for all the other cases it is V.

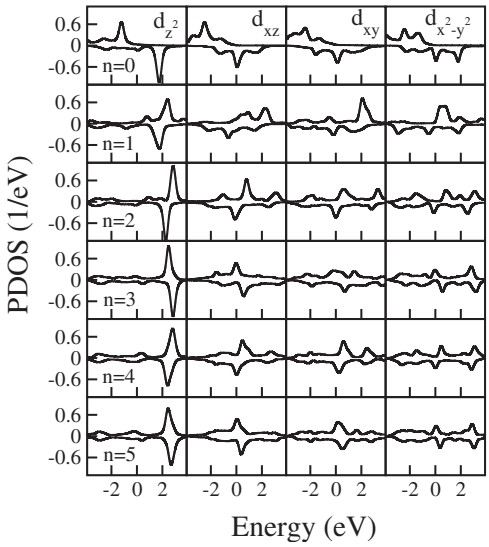

FIG. 12. Density of states projected onto the 3d orbitals of either the Fe($n=0$) or the V($n>0$) layer next to the MgO barrier for the P configuration of the Fe electrodes in the Fe/V_n/MgO/Fe MTJ. Panels on the same row correspond to the same n. The PDOSs, respectively, of the d_{z^2} (Δ_1 symmetry), d_{xz} (Δ_5), d_{xy} (Δ_2), and $d_{x^2-y^2}$ (Δ_2) orbitals are shown from left to right. The PDOS of the d_{yz} orbital is identical to that of the d_{xz} and it is not displayed. Positive and negative PDOSs are for majority and minority spins, respectively.

barrier are calculated and presented in Fig. 12. In the standard Fe/MgO/Fe MTJ, the PDOS for the minority electrons of Fe nearest to MgO shows evidence of interface states and the PDOS peaks at E_F. When a single layer of V is inserted at the Fe/MgO interface, the interface states are severely suppressed. However, for an even number of V layers, the interface states of the minority electrons reappear at the Fermi energy, this time due to V. In contrast, for an odd number of V layers are the majority electrons to show evidence of interface states at E_F as a consequence of the magnetization reversal. This electronic structure correlates well with the conductance oscillations upon increasing the number of V layers, thus we can conclude that the conductance oscillations result from the change in interface states with increasing V layers.

A second notable feature of Fig. 12 is the reduction in exchange splitting (the separation between peaks in the majority and minority PDOSs) as the number of V layers increases. For example, the exchange splitting of V in Fe/V_n/MgO/Fe MTJ with $n=4$ is reduced to about half of that of $n=2$. This observation is consistent with the decrease in the V moment at the V/MgO interface from about μ_B for $n=2$ to about $0.5\mu_B$ for $n=4$. Other relevant aspects of Fig. 12 are the absence of interface states at E_F for $n=1$ and the fact that in all cases the Δ_5 (d_{xz} and d_{yz}) interface states have the most pronounced amplitude at E_F and the Δ_1 (d_{3z^2}) the smallest. This last feature seems to agree well with attributing the increase in conductance originating from the 2D BZ edges as V is intercalated to electrons with Δ_5 symmetry. Notice that the band structure of bulk V presented in Fig. 1 is the extreme case, where only Δ_5 are present at the Fermi level, therefore the Δ_1 states are absent. This should be valid

TABLE I. Conductances, G, (in unit of e^2/h) and both optimistic and pessimistic TMRs for Fe/V_n/Fe_m/MgO/Fe MTJs. The first column describes the magnetic configuration of the junction. Majority and minority spins are defined with respect of the magnetization of the left-hand side Fe electrode.

MTJ	Configuration	G^{majority} e^2/h	G^{minority} e^2/h	TMR^{opt} (%)	TMR^{pes} (%)
$n=2$,	↑↑↑	4.78×10^{-8}	3.19×10^{-7}	−1200	−93
$m=4$	↑↑↓	3.06×10^{-7}	4.65×10^{-6}		
	↑↓↑	4.50×10^{-6}	4.49×10^{-7}		
	↑↓↓	3.02×10^{-4}	8.41×10^{-7}	−6000	−98
$n=2$,	↑↑↑	4.62×10^{-7}	5.66×10^{-4}	11 500	99
$m=6$	↑↑↓	9.89×10^{-7}	3.89×10^{-6}		
$n=4$,	↑↑↑	1.60×10^{-6}	4.49×10^{-4}	4900	98
$m=6$	↑↑↓	5.85×10^{-6}	3.14×10^{-6}		

only for very thick intercalated vanadium layers. In this latter case, the thick vanadium layers play the role of a true barrier to the transport through the Fe Δ_1 states. In all other cases where the V slab is thin, there are some Δ_1 states at the vicinity of the Fermi level at the vanadium site and the interpretation of the transport properties is more difficult.

B. Transport of Fe/V/Fe/MgO/Fe junctions

In Fe/MgO/Fe MTJs, electronic states with Δ_1 symmetry can tunnel through the MgO barrier much easier than the states with Δ_2 and Δ_5 symmetries.[6] One of the main results of the previous sections is that when V is inserted between Fe and MgO, the Δ_1 electrons experience an additional barrier since there are no Δ_1 states at E_F in V. An interesting idea is now to intercalate in the stack a third Fe layer, thus forming a Fe/V_n/Fe_m/MgO/Fe MTJ. It is then expected that the middle Fe layer will act as a quantum well for Δ_1 electrons, which are confined by both V and MgO. A similar type of situation has already been investigated experimentally in Fe/Cr/Fe/MgO/Fe MTJs.[8]

A summary of the calculated transport properties of various Fe/V_n/Fe_m/MgO/Fe MTJs, including the conductances and the TMR, are reported in Table I. In the case when $n=2$ and $m=4$, two magnetic configurations have been considered. These differ by the orientation of the magnetic moment of the middle Fe layer and they are essentially energetically degenerate. As a matter of notation, we indicate a magnetic configuration with α, β, γ where α, β, and γ are the magnetization directions (either ↑ or ↓), respectively, of the left-hand side electrode, the middle Fe layer, and the right-hand side electrode. Thus for the $n=2$ and $m=4$, the ↑↑↑ configuration is only 0.2 meV lower in energy that the ↑↓↑, while ↑↓↓ is 8.9 meV lower than ↑↑↓. Since the V monolayer at V/Fe interface is strongly magnetically coupled to the Fe layer, its direction of magnetization changes depending on that of the intercalated Fe layer.

As shown in Fig. 13, the spin-resolved transmission coefficients are very different depending on the orientation of middle Fe layer, particularly in the energy region around E_F. Thus the conductance of the ↑↑↑ configuration is $3.67\times10^{-7}e^2/h$ against $4.95\times10^{-6}e^2/h$ of the ↑↓↑ state and that of the ↑↑↓ configuration is $4.95\times10^{-6}e^2/h$ against $3.02\times10^{-4}e^2/h$ of the ↑↓↓. Importantly the ratios between the total conductances of configuration that differ only by the direction of the middle layer are 13 and 61 for the P and AP configuration of the Fe electrodes, respectively. This means that the TMR obtained by switching the magnetization of the middle Fe layer only, while keeping those of the electrodes fixed, are 12 and 60 for the P and AP configurations of the Fe electrodes. If the magnetizations of the two Fe electrodes are pinned, e.g., by exchange bias, the magnetization of the middle Fe layers can be reversed with a small magnetic field, leading to a sudden change in conductance. This large sensitivity may be employed to design new spin valves and magnetic-field sensors.

An even more spectacular result is obtained by considering the fact that in the AP configuration of the Fe electrodes, also the magnetization of the middle Fe layers is reversed, since, as mentioned above, the ↑↓↓ configuration is lower in

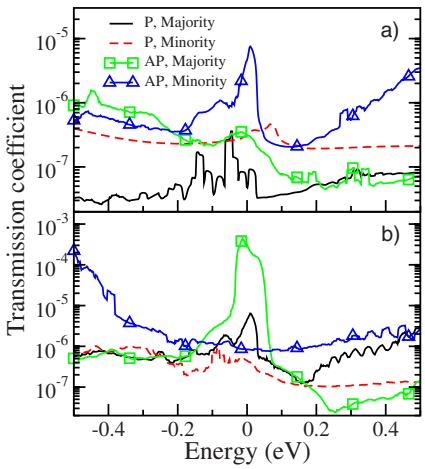

FIG. 13. (Color online) The transmission coefficient of a Fe/V_n/Fe_m/MgO/Fe MTJ in two nearly degenerate magnetic configurations. The V and middle Fe are $n=2$ and $m=4$ monolayers thick, respectively. The magnetization of the middle Fe layers is either parallel (panel a) or antiparallel (panel b) to that of left electrode. P and AP in the legend denote parallel and antiparallel configurations of the Fe electrodes.

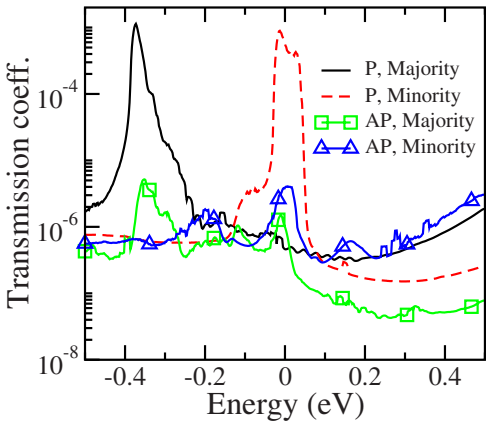

FIG. 14. (Color online) The transmission coefficient of a $Fe/V_n/Fe_m/MgO/Fe$ MTJ with $n=2$ and $m=6$. For both the P and AP configurations of the Fe electrodes, the magnetization of the V layer is antiparallel to that of left-hand side electrode, while that of the intercalated Fe layer is parallel. P and AP in the figure denote the parallel and antiparallel configurations of the Fe electrodes.

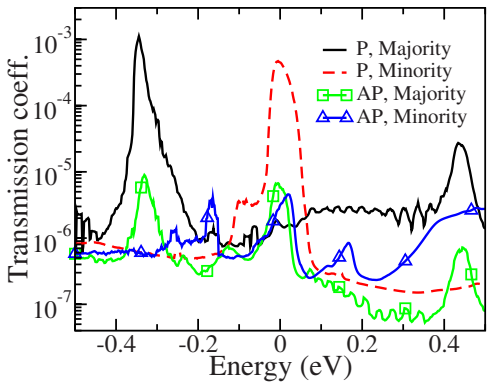

FIG. 15. (Color online) The transmission coefficient of a $Fe/V_n/Fe_m/MgO/Fe$ MTJ with $n=4$ and $m=6$. For both the P and AP configurations of the Fe electrodes, the magnetization of the V layer is antiparallel to that of left-hand side electrode, while that of the intercalated Fe layer is parallel. P and AP in the figure denote the parallel and antiparallel configurations of the Fe electrodes.

energy than the $\uparrow\uparrow\uparrow$ one. If now we calculate the zero-bias TMR obtained by using the conductances of these two states, we obtain a huge value 822 000% (using the optimistic definition). Note that this is the signal expected for a conventional TMR experiment, where the orientation of the electrodes is changed although such a huge value is a consequence of the rearrangement of the internal magnetic structure of the MTJ (the simultaneous switch of the middle Fe layer).

The effects of changing the thickness of the V and the intercalated Fe layers are now explored. We have seen in Fig. 6 that when the number of vanadium layers n are even, the ground state of the interface shows that the vanadium closer to the MgO has a magnetic moment pointing down, whereas when n is odd the magnetic moment is pointing up. In order to get the intercalated Fe quantum-well states magnetic moment parallel to that of the Fe left lead, we should choose even values of n. This will make the tunneling across the V layers more favorable. We did not study the case when n is odd, which should also be interesting since a magnetic field could be used to switch the magnetic moment of the intercalated Fe layers.

We considered first the situation where n is maintained fixed ($n=2$) but m is changed from 4 to 6. Note that for $n=2$ and $m=6$, there is only one stable magnetic configuration with the magnetization of the intercalated Fe layer pinned to that of the left-hand side electrode. The spin-polarized transmission coefficients as a function of energy are presented in Figs. 13 and 14 for $m=4$ and $m=6$, respectively, and the calculated conductances are in Table I. The most evident feature is the massive increase in the minority conductance for the $\uparrow\uparrow\uparrow$ configuration when going from $m=4$ to $m=6$ (from 3.13×10^{-7} to $5.66\times10^{-4}e^2/h$). This, in turn, translates in a huge increase in the absolute value of the TMR, value of TMR for the optimistic definition goes from 1200% to 11 500%. Note that for $m=4$, the TMR is negative, so that the normalizing current in Eq. (2) is actually that of the P configuration. Such a large change in transport properties is a direct consequence of the change in the quantum-well states of the intercalated Fe layer. In particular, the peak in transmission for the minority spins in the parallel configuration for the case $n=2$ and $m=6$ is attributed to a Δ_1 resonance across the Fe intercalated layer. Such a resonance is removed by changing the Fe layer thickness and disappears entirely for $m=4$.

We now turn our attention to the opposite situation, where m is maintained fixed ($m=6$) and n is changed from 2 to 4 (see Figs. 14 and 15 and Table I). Note that for both these MTJs, the middle Fe layer maintains its magnetization parallel to that of the left-hand side electrode so that the TMR is the standard one obtained by changing the orientation of the magnetizations of the electrodes. Figures 14 and 15 reveal no qualitative changes in the transmission of all the spin channels when comparing the two MTJs. The pronounced peak in the minority channel of the $\uparrow\uparrow\uparrow$ state is preserved, confirming that the V layer act simply as tunnel barrier to the high-transmission electrons with Δ_1 symmetry. Other differences are associated to more fine details of the electronic structure and produce only quantitative changes in the transport value. In particular, we find a TMR reduction of about 60% when going from $n=2$ to $n=4$ with the sign of TMR remaining positive.

V. CONCLUSION

The interface and transport properties of Fe/MgO/Fe, Fe/V/MgO/Fe, and Fe/V/Fe/MgO/Fe MTJs are investigated with *ab initio* quantum transport methods. In contrast with a previously published work, Bader analysis reveals a charge transfer from Fe to MgO at the Fe/MgO interface of Fe/MgO/Fe MTJs. This also leads to a substantial increase in the Fe magnetic moment at the interface. For Fe/V/MgO/Fe junctions, we have found that the magnetic configuration of the last V monolayer next to the MgO barrier oscillates with the V layer thickness. Importantly, such interface V magne-

tization has profound effects on the transport of the entire junction and oscillations in both the conductance and the TMR are also found. Unfortunately, the energetics of the various magnetic configurations of the V layer indicate the presence of many equally stable configurations separated by tiny barriers. This poses serious concerns about the overall magnetic stability of such devices.

Then we have turned our attention to Fe/V/Fe/MgO/Fe MTJs. The rationale of such devices is that the intercalated Fe layer is sandwiched in between materials (V and MgO) which act as potential barriers for electrons with Δ_1 symmetry so that there is the possibility of creating quantum-well states. These are indeed found and their profound influence on the transport was demonstrated. On the one hand, we have shown that MTJ, where the middle layer can be switched in a magnetic field while maintaining fixed the magnetization of the electrodes, may display huge TMRs. On the other hand we have also demonstrated that such effect is rather sensitive to the thickness of the Fe intercalated layer. This may be an emerging successful concept in the design of MTJ although concerns may be in order since accurate layer-by-layer deposition may be required to produce high throughput devices.

ACKNOWLEDGMENTS

The calculations were performed using the CINES IBM SP4 supercomputer under Computer Grant No. gem1100. X.F., O.B., and M.A. would like to acknowledge funding support from the ANR of France Grant No. ANR-06-NANO-053-01. The SMEAGOL project (I.R. and S.S.) was sponsored by Science Foundation of Ireland (Grants No. 07/IN.1/I945 and No. 07/RFP/PHYF235). We would also like to thank S. Lebegue for helping with the VASP calculations.

[1] T. Miyazaki and N. Tezuka, J. Magn. Magn. Mater. **139**, L231 (1995).
[2] J. S. Moodera, L. R. Kinder, T. M. Wong, and R. Meservey, Phys. Rev. Lett. **74**, 3273 (1995).
[3] M. Julliere, Phys. Lett. **54A**, 225 (1975).
[4] C. Heiliger, P. Zahn, and I. Mertig, Mater. Today **9**, 46 (2006).
[5] C. Tiusan, F. Greullet, M. Hehn, F. Montaigne, S. Andrier, and A. Schuhl, J. Phys.: Condens. Matter **19**, 165201 (2007).
[6] W. H. Butler, X.-G. Zhang, T. C. Schulthess, and J. M. MacLaren, Phys. Rev. B **63**, 054416 (2001).
[7] J. M. MacLaren, X.-G. Zhang, and W. H. Butler, Phys. Rev. B **56**, 11827 (1997).
[8] F. Greullet, C. Tiusan, F. Montaigne, M. Hehn, D. Halley, O. Bengone, M. Bowen, and W. Weber, Phys. Rev. Lett. **99**, 187202 (2007).
[9] X.-G. Zhang and W. H. Butler, Phys. Rev. B **70**, 172407 (2004).
[10] S. Yuasa, T. Nagahama, A. Fukushima, R. Suzuki, and K. Ando, Nature Mater. **3**, 868 (2004).
[11] S. S. P. Parkin, C. Kaiser, A. Panchula, P. M. Rice, B. Hughes, M. Samant, and S.-H. Yang, Nature Mater. **3**, 862 (2004).
[12] S. Yuasa, A. Fukushima, H. Kubota, Y. Suzuki, and K. Ando, Appl. Phys. Lett. **89**, 042505 (2006).
[13] Y. M. Lee, J. Hayakawa, S. Ikeda, F. Matsukura, and H. Ohno, Appl. Phys. Lett. **90**, 212507 (2007).
[14] T. Nagahama, S. Yuasa, E. Tamura, and Y. Suzuki, Phys. Rev. Lett. **95**, 086602 (2005).
[15] S. Yuasa, T. Nagahara, and Y. Suzuki, Science **297**, 234 (2002).
[16] K. D. Belashchenko, J. Velev, and E. Y. Tsymbal, Phys. Rev. B **72**, 140404(R) (2005).
[17] K. Tsunekawa, D. D. Djayaprawira, S. Yuasa, M. Nagai, H. Maehara, S. Yamagata, E. Okada, N. Watanabe, Y. Suzuki, and K. Ando, IEEE Trans. Magn. **42**, 103 (2006).
[18] A. R. Rocha, V. M. Garcia-Suarez, S. Bailey, C. Lambert, J. Ferrer, and S. Sanvito, Nature Mater. **4**, 335 (2005).
[19] A. R. Rocha, V. M. Garcia-Suarez, S. Bailey, C. Lambert, J. Ferrer, and S. Sanvito, Phys. Rev. B **73**, 085414 (2006).
[20] I. Rungger and S. Sanvito, Phys. Rev. B **78**, 035407 (2008).
[21] R. Landauer, IBM J. Res. Dev. **1**, 233 (1957).
[22] R. Landauer, Philos. Mag. **21**, 863 (1970).
[23] M. Büttiker, Phys. Rev. Lett. **57**, 1761 (1986).
[24] L. P. Kadanoff and G. Baym, *Quantum Statistical Mechanics* (Benjamin/Cummings, New York, 1962).
[25] L. V. Keldysh, Sov. Phys. JETP **20**, 1018 (1965).
[26] Y. Meir and N. S. Wingreen, Phys. Rev. Lett. **68**, 2512 (1992).
[27] S. Datta, *Electronic Transport in Mesoscopic Systems* (Cambridge University Press, Cambridge, England, 1995).
[28] H. Haug and A. P. Jauho, *Quantum Kinetics in Transport and Optics of Semiconductors* (Springer-Verlag, Berlin, 1996).
[29] J. P. Perdew, K. Burke, and M. Ernzerhof, Phys. Rev. Lett. **77**, 3865 (1996).
[30] P. Ordejon, E. Artacho, and J. M. Soler, Phys. Rev. B **53**, R10441 (1996).
[31] J. Soler, E. Artacho, J. D. Gale, A. Garcia, J. Junquera, P. Ordejon, and D. Sanchez-Portal, J. Phys.: Condens. Matter **14**, 2745 (2002).
[32] R. Bader, *Atoms in Molecules: A Quantum Theory* (Oxford University Press, New York, 1990).
[33] G. Henkelman, A. Arnaldsson, and H. Jónsson, Comput. Mater. Sci. **36**, 354 (2006).
[34] E. Sanville, S. D. Kenny, R. Smith, and G. Henkelman, J. Comput. Chem. **28**, 899 (2007).
[35] X.-G. Zhang and W. H. Butler, J. Phys.: Condens. Matter **15**, R1603 (2003).
[36] G. Kresse and J. Hafner, Phys. Rev. B **47**, 558 (1993).
[37] G. Kresse and J. Hafner, Phys. Rev. B **49**, 14251 (1994).
[38] G. Kresse and J. Furthmüller, Comput. Mater. Sci. **6**, 15 (1996).
[39] G. Kresse and J. Furthmüller, Phys. Rev. B **54**, 11169 (1996).
[40] P. E. Blöchl, Phys. Rev. B **50**, 17953 (1994).
[41] G. Kresse and D. Joubert, Phys. Rev. B **59**, 1758 (1999).
[42] J. P. Perdew, J. A. Chevary, S. H. Vosko, K. A. Jackson, M. R. Pederson, D. J. Singh, and C. Fiolhais, Phys. Rev. B **46**, 6671 (1992).
[43] C. W. M. Castleton, S. Nokbin, and K. Hermansson, J. Phys.: Conf. Ser. **100**, 082027 (2008).
[44] J. Izquierdo, A. Vega, O. Elmouhssine, H. Dreyssé, and C. Demangeat, Phys. Rev. B **59**, 14510 (1999).

[45] D. Iusan, M. Alouani, O. Bengone, and O. Eriksson, Phys. Rev. B **75**, 024412 (2007).
[46] I. Rungger, A. R. Rocha, O. Mryasov, O. Heinonen, and S. Sanvito, Mater. Res. Soc. Symp. Proc. **941E**, 0941–Q01–03 (2006).
[47] I. Rungger, A. R. Rocha, O. Mryasov, O. Heinonen, and S. Sanvito, J. Magn. Magn. Mater. **316**, 481 (2007).
[48] I. Rungger, O. Mryasov, and S. Sanvito, Phys. Rev. B **79**, 094414 (2009).